PROGRESSIVE PSEUDOGRAIN DAMAGE MODEL OF SHORT-FIBER REINFORCED PLASTICS FOR PREDICTING THEIR FATIGUE LIFE

J. Yang[1], J. Choi[1], J. Jang[1], H. Pang[1], J.-M. Cho[2], and W.-R. Yu[1]*

[1] Department of Materials Science and Engineering (MSE) and Research Institute of Advanced Materials (RIAM), Seoul National University, Seoul 08826, Republic of Korea
[2] R&D Division, Hyundai Motor Company, Hwaseong-si 18280, Republic of Korea
* Corresponding author (woongryu@snu.ac.kr)

Keywords: Short fiber-reinforced plastics, Two-step homogenization, Fatigue life prediction

ABSTRACT

A progressive pseudograin damage accumulation (PPDA) model for predicting the fatigue life of short fiber-reinforced plastics (SFRPs) is proposed. The model combines viscoelastic-viscoplastic (VEVP) two-step homogenization theory with the Chaboche fatigue damage model. The SFRP's representative volume element (RVE) is decomposed into pseudograins using a machine learning-assited two-step homogenization framework. Then, the fatigue life of each pseudograin is predicted using a master S-N curve prepared based on so called “normalized fatigue factor” that considers stress ratio and multi-axial stress state. Thereafter, the overall failure of RVE is predicted by PPDA model. Each pseudograin fails progressively, resulting in non-linear fatigue damage evolution and stress concentration of the other living pseudograins. The model is implemented in ABAQUS user material subroutine (UMAT) and fatigue lifetime predicted by UMAT was in a good agreement with experimental data.

1 INTRODUCTION

Short fiber-reinforced plastics (SFRPs) have been widely used in automotive, aerospace and construction field due to their low density and high strength [1]. Injection-molded short fiber-reinforced plastics (SFRPs) offer benefits in terms of molding flexibility, cycle time, and formability. However, when used in structural parts, SFRPs are often subjected to multiaxial fatigue loading under dynamic environmental conditions. To effectively design SFRP parts and minimize the costs associated with time-consuming fatigue experiments, an efficient numerical modeling method is needed.

Various fatigue failure models of SFRPs have been reported. Phenomenological models describe the fatigue behavior of SFRPs at a macroscopic level [2, 3]. these models require extensive experimental characterization of fatigue properties, particularly when the properties of constituent materials, such as fiber volume fraction, aspect ratio or orientation tensor, vary significantly [4, 5]. This makes it difficult to apply phenomenological models to predict the fatigue behavior of SFRP parts with complex local fiber orientations and significant differences in mechanical properties. Micromechanical models described the fatigue failure of SFRPs taking account for individual constituents. Researchers described micromechanical models considering matrix damage [6] and delamination [7]. However, micromechanical models are computationally expensive.

Pierard et al. [8] proposed a two-step homogenization framework that allows for the consideration of constituent material properties at an affordable computational cost. To describe non-linear behavior of SFRPs, viscoelastic-viscoplastic (VEVP) matrix and elastic fiber was also proposed [9] and developed [10]. Kammoun et al. [11] extended this framework with a pseudograin damage accumulation model. Rather than defining the overall failure of whole composites, a progressive failure is modeled as successive failures of pseudograins, employing continuum damage mechanics to calculate the damage accumulation of each pseudograin. The “first pseudograin damage (FPGD)” model by analogy with first-ply-failure concept for laminates was used to predict static failure of SFRPs under tensile loading considering multiaxial loading with various fiber orientations. However, it only predicts the static failure of SFRPs, not fatigue failure. Krairi et al. [12] proposed a fatigue failure prediction model of SFRPs using mean-field homogenization method. This model assigned a continuum damage evolution law to weak spots in the SFRPs and calculated the damage evolution using the matrix strain. However, the volume fraction and damage parameters of the weak spot are assumed to be the value estimated through reverse engineering of the S-N curve.

In this study, we propose a new model called 'the progressive pseudograin damage accumulation (PPDA)' model which is capable of predicting the fatigue life of short fiber-reinforced plastics. In our proposed model, multiaxiality and stress ratio effect of pseudograin is considered using a so called "normalized fatigue factor". The overall failure of SFRPs is predicted by PPDA model considering the stress concentration and fatigue damage of pseudograins. Finally, PPDA model is implemented into ABAQUS user material subroutine (UMAT) and validated with experimental results.

2 THEORY

2.1 Viscoelastic-viscoplastic model for matrix

2.1.1 Linear viscoelastic model

The increment in overall strain can be decomposed into two components: a viscoelastic strain increment $d\boldsymbol{\varepsilon}^{ve}$ and a viscoplastic strain increment $d\boldsymbol{\varepsilon}^{vp}$.

$$d\boldsymbol{\varepsilon} = d\boldsymbol{\varepsilon}^{ve} + d\boldsymbol{\varepsilon}^{vp} \tag{1}$$

To calculate the linear viscoelastic stress, the Boltzmann superposition principle is utilized in integral form [13].

$$\boldsymbol{\sigma}(t) = \int_{-\infty}^{t} \mathbf{C}^{ve}(t-\tau) : \frac{\partial \boldsymbol{\varepsilon}^{ve}}{\partial \tau} d\tau \tag{2}$$

where $\mathbf{C}^{ve}(t)$ and $\mathbf{C}^{ve}_{\infty}$ are relaxation tensor and long-term relaxation tensor written as:

$$\mathbf{C}^{ve}(t) = 2G(t)\mathbf{I}^{dev} + 3K(t)\mathbf{I}^{vol} \tag{3}$$

$$\mathbf{C}^{ve}_{\infty} = 2G_{\infty}\mathbf{I}^{dev} + 3K_{\infty}\mathbf{I}^{vol} \tag{4}$$

where $\mathbf{I}^{vol}$ and $\mathbf{I}^{dev}$ are the volumetric and deviatoric operators, respectively. They can be expressed as: $\mathbf{I}^{vol} \equiv \frac{1}{3}\mathbf{1}\otimes\mathbf{1}$ and $\mathbf{I}^{dev} \equiv \mathbf{I} - \mathbf{I}^{vol}$, where $\mathbf{1}$ and $\mathbf{I}$ are the second and the fourth order symmetric identity tensors, respectively. The shear and bulk stiffness, denoted by $G(t)$ and $K(t)$ respectively, can be represented as Prony series:

$$\begin{cases} G(t) = G_{\infty} + \sum_{j=1}^{N} G_j \exp(-\frac{t}{g_j}) \\ K(t) = K_{\infty} + \sum_{j=1}^{N} K_j \exp(-\frac{t}{k_j}) \end{cases} \tag{5}$$

G_{∞} and K_{∞} represent the long-term relaxation moduli. N is the number of Maxwell elements. G_j and K_j are the relaxation weights, and g_j and k_j are the relaxation times.

2.1.2 Viscoplastic model

The Perzyna viscoplastic flow rule is used for viscoplastic behavior.

$$\dot{\boldsymbol{\varepsilon}}^{vp} = \dot{\gamma}\mathbf{N} = \dot{\gamma}\frac{\partial f}{\partial \boldsymbol{\sigma}}, \ \dot{\gamma} = \frac{\sigma_{y0}}{\mu}\left\langle \left(\frac{f}{\sigma_{y0}}\right)^{m} \right\rangle \tag{6}$$

where $\frac{\partial f}{\partial \boldsymbol{\sigma}}$ indicates the direction of viscoplastic strain vector perpendicular to the yield surface in the flow rule. $\dot{\gamma}$ is the viscoplastic multiplier indicating the magnitude of the viscoplastic strain vector. μ and m are viscosity coefficient and exponent, respectively. In the above equation, "$\langle \bullet \rangle$" are MacCauley brackets used to describe $\langle \bullet \rangle = 0$ when $\bullet < 0$, and $\langle \bullet \rangle = \bullet$ when $\bullet \geq 0$. Isotropic hardening stress function with power law is used for yield function as follows:

$$f = \bar{\sigma} - \sigma_{y0} - \kappa(\bar{\varepsilon}^{vp}) \tag{7}$$

$$\kappa(\bar{\varepsilon}^{vp}) = A(\bar{\varepsilon}^{vp})^{B} \tag{8}$$

where σ_{y0} is initial yield strength and $\kappa(\bar{\varepsilon}^{vp})$ is isotropic hardening stress function. In this model, equivalent stress $\bar{\sigma}$ is calculated using classical J2 theory (von Mises stress). A and B are hardening coefficient and exponent, respectively.

2.2 Pseudograin stress

In order to calculate the stress tensor of every pseudograin, the homogenization of elastic fiber and VEVP matrix is required. Mean-field homogenization method based on the Mori-Tanaka model is used [8]. Herein, we briefly introduce mean-field homogenization between elastic fiber and VEVP matrix. The macro-strain field is expressed as $\langle \boldsymbol{\varepsilon} \rangle_{\Omega}$, where $\langle \bullet \rangle_{\Omega}$ designates volume averaging operator quantity. The average micro-strain field in each phase can be correlated using the strain concentration tensor (between matrix and fiber) $\mathbf{A}^{\varepsilon}$ as follows.

$$\langle \boldsymbol{\varepsilon} \rangle_{\Omega_f} = \mathbf{A}^{\varepsilon} : \langle \boldsymbol{\varepsilon} \rangle_{\Omega_m} \tag{9}$$

Mori-Tanaka model assumes that all fibers in composites are aligned and identical. The strain concentration tensor $\mathbf{A}^{\varepsilon}$ provided by the Mori–Tanaka model is as follows:

$$\mathbf{A}^{\varepsilon} = \left[\mathbf{I} + \mathbf{S} : (\mathbf{C}_m^{-1} : \mathbf{C}_f - \mathbf{I}) \right]^{-1} \tag{10}$$

where S is Eshelby's tensor of ellipsoidal inclusion. The details of the Eshelby's tensor component are given in Mura's study [14]. Average macro-strain field can be correlated using the strain concentration tensor (between phase and macro-strain) $\mathbf{B}^{\varepsilon}$ are as follows:

$$\mathbf{B}_m^{\varepsilon} = \left[v_m \mathbf{I} + v_f \mathbf{A}^{\varepsilon} \right]^{-1},\ \mathbf{B}_f^{\varepsilon} = \mathbf{A}^{\varepsilon} \left[v_m \mathbf{I} + v_f \mathbf{A}^{\varepsilon} \right]^{-1} \tag{11}$$

where v_m and v_f are the volume fraction of matrix phase and fiber phase, respectively. Strain increment field of macroscopic composites, fiber and matrix phases are proposed by Doghri et al. [15] as follows:

$$\langle \Delta\boldsymbol{\varepsilon} \rangle_{\Omega} = v_m \langle \Delta\boldsymbol{\varepsilon} \rangle_{\Omega_m} + v_f \langle \Delta\boldsymbol{\varepsilon} \rangle_{\Omega_f} \tag{12}$$

$$\langle \Delta\boldsymbol{\varepsilon} \rangle_{\Omega_f} = \mathbf{B}_f : \langle \Delta\boldsymbol{\varepsilon} \rangle_{\Omega} + (\mathbf{I} - \mathbf{B}_f) : (\mathbf{C}_m - \mathbf{C}_f)^{-1} : \langle \Delta\boldsymbol{\tau} \rangle_{\Omega_m} \tag{13}$$

$$\langle \Delta\boldsymbol{\varepsilon} \rangle_{\Omega_m} = \mathbf{B}_m : \langle \Delta\boldsymbol{\varepsilon} \rangle_{\Omega} - \frac{v_f}{v_m} (\mathbf{I} - \mathbf{B}_f) : (\mathbf{C}_m - \mathbf{C}_f)^{-1} : \langle \Delta\boldsymbol{\tau} \rangle_{\Omega_m} \tag{14}$$

where $\Delta\boldsymbol{\tau}$ is the increment of inelastic term. The increment of inelastic term is calculated by incrementally affine linearization method developed by Miled et al. [9]. The VEVP stress increment of the matrix can be linearized with tangent stiffness $\mathbf{C}_m$ and inelastic term $\Delta\boldsymbol{\tau}$ as follows:

$$\Delta\boldsymbol{\sigma} = \mathbf{C}_m : \Delta\boldsymbol{\varepsilon} + \Delta\boldsymbol{\tau} \tag{15}$$

Substituting Equation (13) and (14) into Equation (12) with respect to the stress increment field, we obtain,

$$\langle \Delta\boldsymbol{\sigma} \rangle_{\Omega} = \langle \mathbf{C} \rangle_{\Omega} : \langle \Delta\boldsymbol{\varepsilon} \rangle_{\Omega} + v_f (\mathbf{C}_f - \mathbf{C}_m) : (\mathbf{I} - \mathbf{B}_f) : (\mathbf{C}_m - \mathbf{C}_f)^{-1} : \langle \Delta\boldsymbol{\tau} \rangle_{\Omega_m} \tag{16}$$

$\langle \mathbf{C} \rangle_{\Omega}$ is the effective stiffness tensor of macroscopic composites is derived as follows:

$$\langle \mathbf{C} \rangle_{\Omega} = \left[v_m \mathbf{C}_m + v_f \mathbf{C}_f : \mathbf{A}^{\varepsilon} \right] : \mathbf{B}_m^{\varepsilon} \tag{17}$$

2.3 Fatigue lifetime for each pseudograin

2.3.1 Normalized fatigue factor

Kawai et al. [16] proposed "modified fatigue stress ratio" using Tsai-Hill effective stress (η) and stress ratio (R) for unidirectional continuous fiber-reinforced plastics.

$$\Phi = \frac{1/2(1-R)\eta}{1-1/2(1+R)\eta} \tag{18}$$

In our study, Tsai-Wu effective stress ξ is used instead of η in Equation (18). In addition, Equation (18) is modified to apply to SFRPs. Jang et al [17] modified Equation (18) for SFRPs by introducing the additional term. Using fitting parameter λ_1, a new equation for master S-N curve was suggested in terms of 'normalized fatigue factor (NFF)' and validated by demonstrating that S-N curves of various FRPs can be collapsed into a single master S-N curve using NFF in the followings.

$$\psi = \frac{1/2(1-R)\xi}{1-1/2(1+R)\xi} + \lambda_1 R(1-R)\xi \quad (-1 \le R \le 1) \tag{19}$$

Tsai-Wu failure criteria [18] was used for the effective stress ξ. Assuming that pseudograin is transversely isotropic and that σ_{23} is negligible, Tsai-Wu failure criteria can be expressed as follows:

$$\begin{gathered} TW(\boldsymbol{\sigma}_{ij}) = [F_{11}\boldsymbol{\sigma}_{11}^2 + F_{22}(\boldsymbol{\sigma}_{22}^2 + \boldsymbol{\sigma}_{33}^2) + F_{66}(\boldsymbol{\sigma}_{12}^2 + \boldsymbol{\sigma}_{13}^2)] + [F_1\boldsymbol{\sigma}_{11} + F_2(\boldsymbol{\sigma}_{22} + \boldsymbol{\sigma}_{33})] = 1 \\ F_1 = \frac{1}{X_t} - \frac{1}{X_c},\ F_2 = \frac{1}{Y_t} - \frac{1}{Y_c},\ F_{11} = \frac{1}{X_t X_c},\ F_{22} = \frac{1}{Y_t Y_c},\ F_{66} = \frac{1}{S^2} \end{gathered} \tag{20}$$

In this study, non-dimensional Tsai-Wu effective stress is defined as the distance from origin to the failure envelope, representing the ratio of the magnitude of the current stress state to the static failure of the composites as shown in Figure 1.

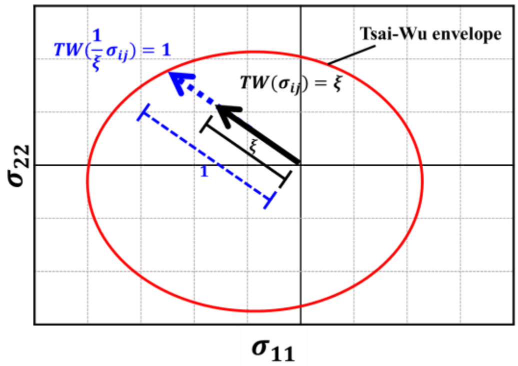

Figure 1. Schematic illustration of non-dimensional Tsai-Wu effective stress.

2.3.2 Chaboche fatigue damage model

After multiaxial stress state of pseudograin is converted to universal scalar quantity (NFF), fatigue damage model is required to predict the lifetime of pseudograins. Chaboche et al. suggested a non-linear continuous fatigue damage model for stress-controlled condition [19]. This model describes the progressive degradation of material for the crack initiation process.

$$\frac{dD}{dN} = [1-(1-D)^{\beta+1}]^{\alpha} \left(\frac{S_{\max} - S_m}{M(1-D)} \right)^{\beta} \tag{21}$$

where D is the fatigue damage variable, $S_{\max}$ is the maximum stress, and S_m is the mean stress, β is constant. α and M are stress dependent functions and are expressed by,

$$\alpha = 1 - a \left\langle \frac{S_{\max} - S_m - S_{10}(1-bS_m)}{S_u - S_{\max}} \right\rangle \tag{22}$$

$$M = M_0(1-bS_m) \tag{23}$$

where S_{l0} is the fatigue limit, S_u is the ultimate tensile strength, a is non-linearity parameter, b is mean stress effect parameter, and M_0 is a constant. This fatigue damage law was used to predict fatigue life of SFRPs by incorporating NFF into Equation (19) as follows.

$$\frac{dD}{dN} = [1-(1-D)^{\beta+1}]^{\alpha} \left(\frac{\psi_{\max}}{M_0(1-D)} \right)^{\beta} \tag{24}$$

Integrating damage from 0 to 1 in Equation (24), fatigue lifetime (N_f) can be expressed as:

$$N_f = \frac{1}{(\beta+1)(1-\alpha)} \left(\frac{\psi_{\max}}{M_0} \right)^{-\beta} \tag{25}$$

2.4 Fatigue lifetime for RVE

In this section, the method to predict the overall failure of RVE is introduced. PPDA model is inspired by the progressive-ply-failure concept of laminate composites [20]. Once a pseudograin fails, the stress of the other pseudograins is concentrated.

We assume that the RVE in the fatigue loading is composed of k pseudograins: PG_i (i=1, 2, …, k). The NNF of pseudograins is calculated to ψ_i (i=1, 2, …, k) by Equation (13). The fatigue life of pseudograins is expressed by $N_{f.i}$ (i=1, 2, …, k) using Equation 20. Here, assume that PG_1 is a pseudograin with the shortest lifetime and PG_k is the pseudograin with the longest lifetime. Once PG_1 has failed first, all pseudgrains are cycled through $N_{f.1}$ cycles. At this cycle ($N_{f.1}$), the stress of the other pseudograins (PG_i) is concentrated by accumulated damage of the other pseudograins. This damage is expressed as follows:

$$D_{i.1} = 1 - \left(1 - \left(\frac{N_{f.1}}{N_{f.i}} \right)^{\frac{1}{1-\alpha}} \right)^{\frac{1}{\beta+1}} \tag{26}$$

where $D_{i.1}$ is accumulated damage in PG_i at $N_{f.1}$ cycles. Using Equation (26), stress concentration due to the failure of PG_1. is determined. The scheme of PPAD model is provided in Figure 2.

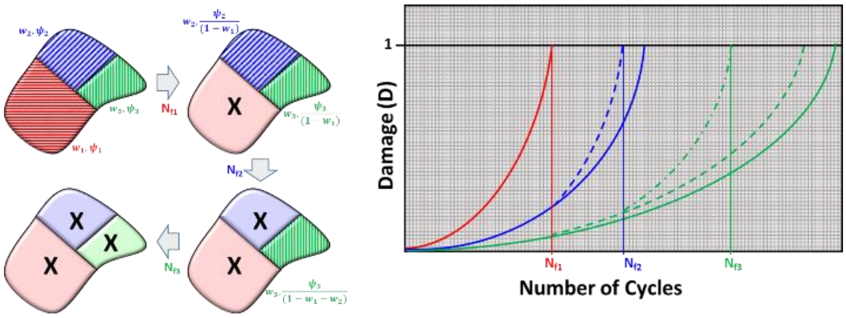

Figure 2. The scheme of progressive damage accumulation method.

3 EXPERIMENTAL

3.1 Materials

SFRP specimens were made of short glass fiber-reinforced polypropylene. The glass fibers with 30% weight fraction was embedded in polypropylene (or 13.09% volume fraction). The injection-molded sheets with a thickness of 2.7 mm were prepared and hereafter denoted by PP-GF30. The fiber orientation tensor a_{ij} used in this study is as follows:

$$a_{ij} = \begin{bmatrix} 0.741 & 0.000 & 0.000 \\ 0.000 & 0.242 & 0.000 \\ 0.000 & 0.000 & 0.017 \end{bmatrix} \tag{27}$$

3.2 Mechanical testing of PP

The VEVP properties of the polypropylene matrix were characterized. The viscoelastic parameters were identified by dynamic mechanical analysis (DMA) test. DMA test machine (Q800, TA instrument, USA) was used. The length and width of specimen were 60 and 10 mm, respectively. Testing temperature were ranged from −50 to 140°C with 10°C increments. The frequency was ranged from 0.01 to 10 Hz. The viscoplastic parameters were obtained by tensile tests. Tensile tests were conducted at room temperature (25°C) using a tensile testing machine (Instron 8801; Instron, Norwood, MA, USA) according to the ISO 527-2 standard [40]. Two test speeds (1.15 and 5 mm/min) were used. A digital image correlation (DIC) system (Vic-3D v7; Correlated Solutions, Inc., Irmo, SC, USA) was used to measure the tensile strain of the specimens. The dog bone-shaped specimens were used. The total length and gauge width of each specimen were 180 and 10 mm, respectively.

3.3 Fatigue testing of SFRP

Load-controlled fatigue tests were conducted using an Instron 8801 (Instron 8801; Instron, Norwood, MA, USA). The frequency was set to 5 Hz. The fatigue test was conducted with a stress ratio of 0.1 and -1 at room temperature (25°C). Specimens were obtained from the injection molded plate. The specimens were then machined at different orientation angles by milling. Specimens with three fiber orientation were used and named as PP-GF30-0D, 20D and 90D, respectively.

4 RESULTS AND DISCUSSION

4.1 VEVP behavior of PP

The VEVP properties of PP matrix obtained from the DMA test and tensile tests are shown in Section 4.1. Figure 3 shows the DMA test and tensile test results of polypropylene. The storage modulus - reduced time curve is shown in Figure 3(a). Fitting the storage modulus - reduced time curve, the viscoelastic parameters were obtained. Viscoplastic parameters were obtained by curve fitting of tensile test results as shown in Figure 3(b). The obtained viscoelastic and viscoplastic parameters of the polypropylene were presented in Table 1.

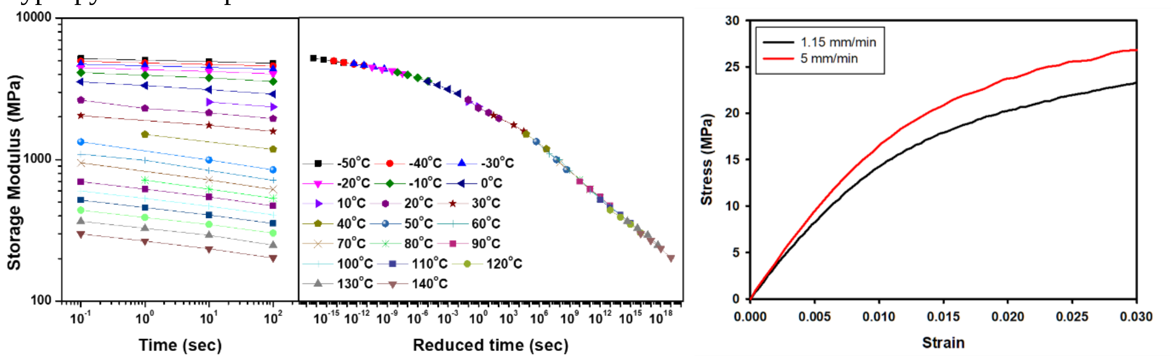

Figure 3. Mechanical tests result of PP: (a) DMA test results and (b) tensile test results.

Viscoelastic parameter		
Instantaneous modulus (E_0)		4201 MPa
j	Relaxation time (τ_j)	Maxwell component moduli ratio (E_j / E_0)
1	10^6	0.0436
2	10^5	0.0475
3	10^4	0.0459

4	10^{3}	0.0268
5	10^{2}	0.0398
6	10^{1}	0.0525
7	10^{0}	0.0361
8	10^{-1}	0.0898
9	10^{-2}	0.0565
10	10^{-3}	0.0511
11	10^{-4}	0.0480
12	10^{-5}	0.0579
13	10^{-6}	0.0455
14	10^{-7}	0.0385
15	10^{-8}	0.0407
Viscoplastic parameter		
Initial yield strength (σ_{y0})		10 MPa
Viscoplasctic coefficient (μ)		5489 MPa·s
Viscoplasctic exponent (m)		1.2
Hardening coefficient (A)		88.79 MPa
Hardening exponent (B)		0.4792

Table 1. VEVP parameters of PP.

4.2 Experimental validation of VEVP homogenization model

shows the re-simulation result for validation of tensile test of PP-GF30. Elastic modulus of 72.40 GPa, Poisson's ratio of 0.22 and fiber aspect ratio of 25 were used for glass fiber in simulation. Poisson's ratio of 0.43 was used for the PP matrix in simulation. A cubic geometry of size 6×6×6 mm was created and meshed with a C3D8 element of size 1×1×1 mm as shown in Figure 4(a). The U1=0, U2=0, and U3=0 boundary conditions were applied to the plane perpendicular to the x-, y-, and z-axis in the negative direction, respectively. A displacement boundary condition of 0.06 mm was applied to the plane perpendicular to the x-axis in the positive direction so that the applied tensile strain was 1%.

The re-simulation result was compared with tensile tests of PP-GF30-0D as shown in Figure 4(b). The simulation result was in good agreement with the experimental stress-strain curve of PP-GF30-0D. It was confirm that the developed UMAT properly described VEVP behavior of SFRPs.

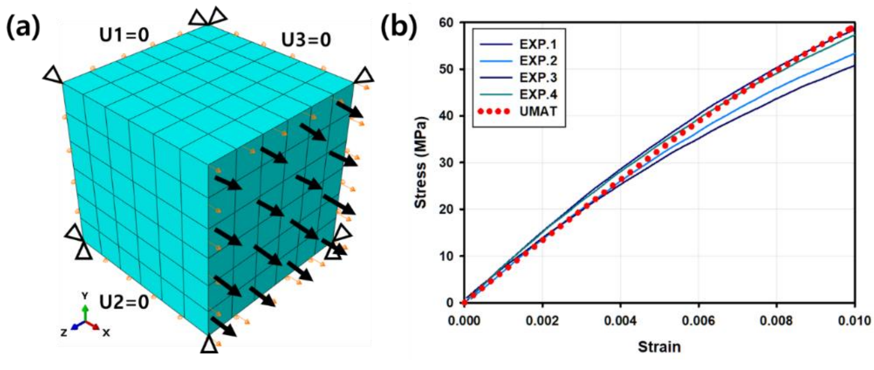

Figure 4. (a) Boundary condition of simulation and (b) experimental and UMAT re-simulation stress–strain curves of PP-GF30-0D

4.3 Experimental validation of PPDA model

The reconstruction of orientation distribution function (ODF) and pseudograin decomposition procedure for 12 pseudograins using machine learning-assisted method were implemented in UMAT. Then, the VEVP model and mean-field homogenization method described in the previous sections were implemented. A cubic geometry of size 6×6×6 mm was created and meshed with a C3D8 element of size 1×1×1 mm. The U1=0, U2=0, and U3=0 boundary conditions were applied to the plane perpendicular to the x-, y-, and z-axis in the negative direction, respectively. A load in a sine wave with

5 Hz frequency was applied to the plane perpendicular to the x-axis in the positive direction. Varying maximum load of sine wave and stress ratio, the fatigue tests of three different specimens (PP-GF30-0D, 20D, 90D) were simulated. Simulation conditions are detailed in Table 2.

Stress ratio (R)	Specimen	Applied maximum stress (MPa)	Applied maximum load (N)
-1	PP-GF30-0D	20, 30, 40, 50, 60	720, 1080, 1440, 1800, 2160
-1	PP-GF30-20D	20, 30, 40, 50	720, 1080, 1440, 1800
-1	PP-GF30-90D	15, 20, 30, 40	540, 720, 1080, 1440
0.1	PP-GF30-0D	40, 50, 60, 70, 80	1440, 1800, 2160, 2520, 2880
0.1	PP-GF30-20D	40, 50, 60, 70	1440, 1800, 2160, 2520
0.1	PP-GF30-90D	40, 50, 60	1440, 1800, 2160

Table 2. (a) Boundary condition of simulation and (b) experimental and UMAT re-simulation stress–strain curves of PP-GF30-0D

The simulation results are presented in Figure 5, where Figure 5(a) and Figure 5(b) show the result of tension-compression ($R=-1$) and tension-tension ($R=0.1$) conditions, respectively. Both S-N curves show a good agreement with experimental results, confirming that NFF reflects the mean stress effect of pseudograins inside SFRPs. The black, red, and green solid lines in Figure 5 represent simulation results of specimens with different fiber orientation tensor (0D, 20D, 90D), showing a good agreement with the experimental results. Therefore, it can be claimed that Tsai-Wu effective stress concept and pseudograin decomposition method can properly capture the effect of fiber orientation. However, there is a slight difference between the simulation results of PP-GF30-0D and PP-GF30-20D in law fatigue cycle (~10^3) shown in Figure 5(a) and the experimental results. This is thought to be due to a master S-N curve fitting problem.

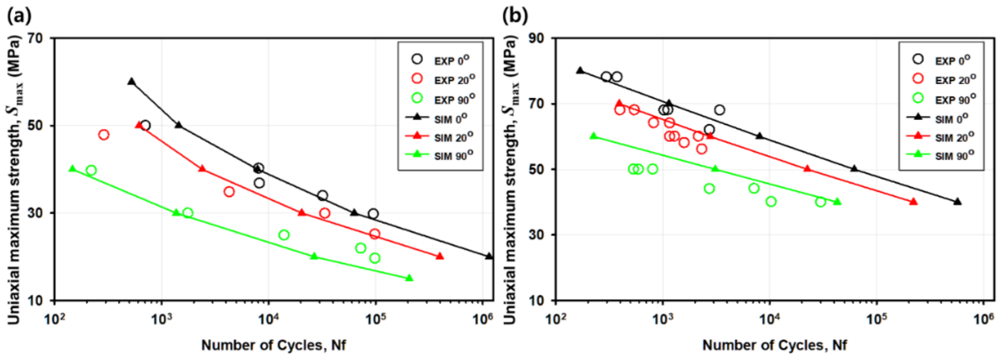

Figure 5. Comparison between numerical and experimental S-N curves of PP-GF30 with different fiber orientations (0D, 20D, 90D) for stress ratio (a) -1 and (b) 0.1.

5 CONCLUSIONS

In this study, we proposed a novel PPDA model to predict fatigue lifetime in SFRPs. Chaboche fatigue damage model was used for the non-linear damage calculation of pseudograins and normalized fatigue factor was used to consider their anisotropic fatigue characteristics. Furthermore, we considered stress concentration and accumulation of fatigue damages. Finally, we determined a reasonable RVE fatigue failure. We implemented PPDA model into UMAT and compared the predicted S-N curves with experimental data. Overall, the proposed model is a promising approach for predicting the fatigue behavior of SFRPs and can potentially be extended to other composite materials.

ACKNOWLEDGEMENTS

This work was supported by the Hyundai Motor Company (0417-20210090) in Republic of Korea. The Institute of Engineering Research at Seoul National University provided research facilities for this work.

REFERENCES

[1]C. Luan, S. Movva, K. Wang, X. Yao, C. Zhang, and B. Wang, Towards next-generation fiber-reinforced polymer composites: a perspective on multifunctionality, *Functional Composites and Structures*, **1**(4), 2019, pp. 042002.
[2]A. Andriyana, N. Billon, and L. Silva, Mechanical response of a short fiber-reinforced thermoplastic: Experimental investigation and continuum mechanical modeling, *European Journal of Mechanics-A/Solids*, **29**(6), 2010, pp. 1065-77.
[3]A. Launay, M. Maitournam, Y. Marco, and I. Raoult, Multiaxial fatigue models for short glass fibre reinforced polyamide. Part II: Fatigue life estimation, *International Journal of Fatigue*, **47**, 2013, pp. 390-406.
[4]M. De Monte, E. Moosbrugger, and M. Quaresimin, Influence of temperature and thickness on the off-axis behavior of short glass fibre reinforced polyamide 6.6–Quasi-static loading, *Composites Part A: Applied Science and Manufacturing*, **41**(7), 2010, pp. 859-71.
[5]M. J. Kanters, L. F. Douven, and P. Savoyat, Fatigue life prediction of injection moulded short glass fiber reinforced plastics, *Procedia Structural Integrity*, **19**, 2019, pp. 698-710.
[6]J. Köbler, N. Magino, H. Andrä, F. Welschinger, R. Müller, and M. Schneider, A computational multi-scale model for the stiffness degradation of short-fiber reinforced plastics subjected to fatigue loading, *Computer Methods in Applied Mechanics and Engineering*, **373**, 2021, pp. 113522.
[7]A. Jain, Y. Abdin, W. Van Paepegem, I. Verpoest, and S. V. Lomov, Effective anisotropic stiffness of inclusions with debonded interface for Eshelby-based models, *Composite Structures*, **131**, 2015, pp. 692-706.
[8]O. Pierard, C. Friebel, and I. Doghri, Mean-field homogenization of multi-phase thermo-elastic composites: a general framework and its validation, *Composites Science and Technology*, **64**(10-11), 2004, pp. 1587-603.
[9]B. Miled, I. Doghri, L. Brassart, and L. Delannay, Micromechanical modeling of coupled viscoelastic–viscoplastic composites based on an incrementally affine formulation, *International Journal of solids and structures*, **50**(10), 2013, pp. 1755-69.
[10]J. Jung, Y. Kim, S. Lee, I. Doghri, and S. Ryu, Improved incrementally affine homogenization method for viscoelastic-viscoplastic composites based on an adaptive scheme, *Composite Structures*, **297**, 2022, pp. 115982.
[11]S. Kammoun, I. Doghri, L. Brassart, and L. Delannay, Micromechanical modeling of the progressive failure in short glass–fiber reinforced thermoplastics–First Pseudo-Grain Damage model, *Composites part A: applied science and manufacturing*, **73**, 2015, pp. 166-75.
[12]A. Krairi, I. Doghri, and G. Robert, Multiscale high cycle fatigue models for neat and short fiber reinforced thermoplastic polymers, *International Journal of Fatigue*, **92**, 2016, pp. 179-92.
[13]M. Kaliske, and H. Rothert, Formulation and implementation of three-dimensional viscoelasticity at small and finite strains, *Computational Mechanics*, **19**(3), 1997, pp. 228-39.
[14]T. Mura, Micromechanics of defects in solids: Springer Science & Business Media; 2013.
[15]I. Doghri, L. Adam, and N. Bilger, Mean-field homogenization of elasto-viscoplastic composites based on a general incrementally affine linearization method, *International Journal of Plasticity*, **26**(2), 2010, pp. 219-38.
[16]M. Kawai, S. Yajima, A. Hachinohe, and Y. Takano, Off-axis fatigue behavior of unidirectional carbon fiber-reinforced composites at room and high temperatures, *Journal of Composite Materials*, **35**(7), 2001, pp. 545-76.
[17]장진혁, Predictive method of fatigue properties of fiber reinforced plastics considering damage: 서울대학교 대학원; 2021.
[18]S. W. Tsai, and E. M. Wu, A general theory of strength for anisotropic materials, *Journal of composite materials*, **5**(1), 1971, pp. 58-80.
[19]J. Chaboche, and P. Lesne, A non-linear continuous fatigue damage model, *Fatigue & fracture of engineering materials & structures*, **11**(1), 1988, pp. 1-17.
[20]Z. Fawaz, and F. Ellyin, A new methodology for the prediction of fatigue failure in multidirectional fiber-reinforced laminates, *Composites science and technology*, **53**(1), 1995, pp. 47-55.